
Visualizing Representations of Adversarially Perturbed Inputs

Daniel Steinberg

Intelligent Systems Program
University of Pittsburgh
das178@pitt.edu

Paul Munro

School of Computing and Information
University of Pittsburgh
pwm@pitt.edu

Abstract

It has been shown that deep learning models are vulnerable to adversarial attacks. We seek to further understand the consequence of such attacks on the intermediate activations of neural networks. We present an evaluation metric, POP- N , which scores the effectiveness of projecting data to N dimensions under the context of visualizing representations of adversarially perturbed inputs. We conduct experiments on CIFAR-10 to compare the POP-2 score of several dimensionality reduction algorithms across various adversarial attacks. Finally, we utilize the 2D data corresponding to high POP-2 scores to generate example visualizations.

Code is available at <https://github.com/dstein64/vrapi>.

1 Introduction

Neural network research has progressed for many decades. Advancements in computing hardware and model training techniques along with a proliferation of data has led to widespread adoption of deep learning for solving an assortment of machine learning problems. Along with its success it has been shown that deep learning models are susceptible to adversarial attacks [SZS⁺14], carefully crafted perturbations of input instances that appear unaltered to humans and cause incorrect model output.

Existing work seeks to 1) develop attack methods [KGB17], 2) develop defense techniques [MMS⁺19], and 3) provide insights on the characteristics of adversarial perturbations and their effects on target networks [MLW⁺18, XLZ⁺19, TV16]. For a broad overview of the field, see [AM18]. Our work—part of the third aforementioned category—is motivated by trying to understand how adversarial attacks effect change on the hidden layer representations of their target networks.

Visualizations have been used to help understand high dimensional data. In this paper, we focus our attention on visualizing representations of adversarial inputs at the penultimate layer of the target network. Dimensionality reduction permits high dimensional data to be projected to 2D, providing data for a scatter plot. The nature of the task presents a challenge to determine how well the projected data preserves the high dimensional structure.

Our contribution In Section 3 we propose the POP-2 score that can be used for evaluating dimensionality reduction algorithms under the context of visualizing representations of adversarially perturbed images. We run experiments in Section 4 comparing several algorithms on CIFAR-10 and present examples of generated visualizations.

2 Preliminaries

We are interested in l -layer feedforward neural networks, which are functions $h : \mathcal{X} \rightarrow \mathcal{Y}$ that map an input $x \in \mathcal{X}$ to output $\hat{y} \in \mathcal{Y}$ through linear preactivation functions f_i and nonlinear activation functions ϕ_i .

$$\hat{y} = h(x) = \phi_l \circ f_l \circ \phi_{l-1} \circ f_{l-1} \circ \dots \circ \phi_1 \circ f_1(x)$$

We focus here on classification problems, where the output of the neural network is a discrete label. For an input x and its true class label y , we denote $J(x, y)$ as the corresponding loss of a trained neural network. For convenience, we omit the dependence on model parameters θ .

2.1 Adversarial Attacks

Consider an input x that is correctly classified by neural network h . For an untargeted adversarial attack, an adversary seeks to devise a small additive perturbation Δx such that adversarial input $x^{adv} = x + \Delta x$ changes the classifier’s output, i.e., $h(x) \neq h(x^{adv})$. Often the L_p norm of Δx is constrained to be smaller than some specified value ϵ . A targeted adversarial attack additionally specifies a desired value for $h(x^{adv})$.

For example, an untargeted adversarial input x^{adv} can be generated through a process that seeks to maximize the loss function. This formulation could be expressed in terms of a constrained optimization objective as follows.

$$\begin{aligned} \Delta x = \operatorname{argmax}_{\delta} \quad & J(x + \delta, y) \\ \text{subject to} \quad & \|\delta\|_p \leq \epsilon \\ & x + \delta \in \mathcal{X} \end{aligned}$$

There are various ways to formulate the task of generating attacks. An exact computation of Δx is often difficult, thereby entailing that an approximation be employed.

Fast Gradient Sign Method (FGSM) [GSS15] generates adversarial inputs with a perturbation in the approximate direction of the loss function gradient, whereby $\Delta x = \epsilon \cdot \operatorname{sign}(\nabla_x J(x, y))$. The sign function alone constrains the perturbation to an L_∞ norm bound of 1, which is then scaled by ϵ .

Basic Iterative Method (BIM) [KGB17] performs multiple iterations of FGSM with each having a separate gradient update. At each step, $x_t^{adv} = x_{t-1}^{adv} + \alpha \cdot \operatorname{sign}(\nabla_x J(x_{t-1}^{adv}, y))$, with $x_0^{adv} = x$. The L_∞ norm is bounded by α on each iteration, and the final x^{adv} can be constrained to an ϵ -ball of x by clipping x_t^{adv} accordingly at each step.

Carlini & Wagner (CW) [CW17] generates adversarial inputs by using a gradient descent routine to solve $\Delta x = \operatorname{argmin}_{\delta} (\|\delta\|_p + c \cdot f(x + \delta))$ subject to a box constraint on $x + \delta$, where $c > 0$ is a suitable constant and f is a function for which $f(x + \delta) \leq 0$ if and only if the target classifier is successfully attacked. The box constraint can be satisfied with clipping or a change of variables. The most effective f of those considered—in the context of targeted attacks—was found through experimentation. Binary search is used to choose the smallest value of c , a strategy that worked well empirically.

2.2 Dimensionality Reduction

Consider a set of n data points in D dimensions represented with matrix $X \in \mathbb{R}^{n \times D}$. For $d < D$, a dimensionality reduction algorithm finds lower-dimensional $Z \in \mathbb{R}^{n \times d}$ that preserves some notion of the high dimensional dataset’s structure (e.g., pairwise distances). Techniques differ in various ways, including how much weight is given to preserving local versus global structure.

An out-of-sample data point is one that is not included in X . Some dimensionality reduction algorithms natively support the projection of arbitrary D -dimensional out-of-sample data points to d dimensions. Out-of-sample extensions have been proposed for adding support to other models [BPV⁺04].

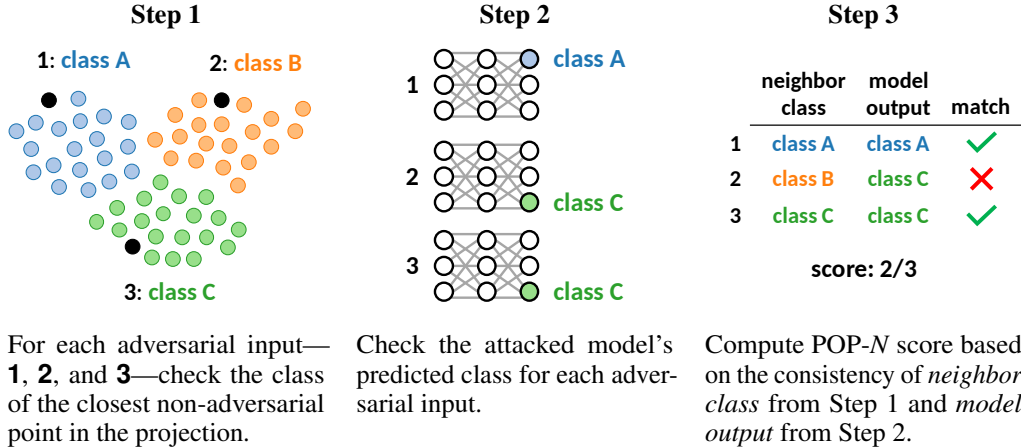


Figure 1: Illustration of the POP- N scoring approach presented in Section 3.

Principal Components Analysis (PCA) [Pea01] is a linear method that finds a lower-dimensional representation of X that maximizes the variance of the projected data. A dual formulation seeks to minimize the sum-of-squared projection errors—the distance of each data point in high dimension to its projection on a lower-dimensional subspace. The optimization problem is solved by computing eigenvalues and eigenvectors of X ’s covariance matrix Σ , often conducted using singular value decomposition (SVD). The d eigenvectors corresponding to the highest eigenvalues are used for transforming D -dimensional data to d dimensions.

t-Distributed Stochastic Neighbor Embedding (t-SNE) [vdMH08] is a dimensionality reduction algorithm designed for visualization. A Gaussian distribution is used for computing normalized pairwise conditional affinity $p_{j|i}$ between points i and j in high dimensional space using a bandwidth parameter σ_i that satisfies a specified perplexity hyperparameter. The asymmetric conditionals $p_{i|j}$ and $p_{j|i}$ are symmetrized to $p_{ij} = (p_{j|i} + p_{i|j}) / (2n)$. An optimization procedure is used to position points in low dimension by minimizing the KL-divergence between p_{ij} and low dimensional normalized pairwise affinity q_{ij} . The formulation of q_{ij} differs from that of p_{ij} , as the former is based on a fatter-tailed Student’s t -distribution instead of a Gaussian, and is not a function of asymmetric conditionals like the latter.

Uniform Manifold Approximation and Projection (UMAP) [MHM20] is a dimensionality reduction technique grounded in manifold theory and topological data analysis, which gives rise to a procedure similar to t-SNE. Pairwise conditional affinity $p_{j|i}$ between points i and j in high dimensional space is calculated as a function of distance between i and j shifted and scaled by local connectivity parameters. The asymmetric conditionals $p_{i|j}$ and $p_{j|i}$ are symmetrized to $p_{ij} = p_{j|i} + p_{i|j} - p_{j|i}p_{i|j}$. An optimization procedure that incorporates negative sampling is used to position points in low dimension by minimizing the cross-entropy between p_{ij} and low dimensional pairwise affinity q_{ij} . The q_{ij} affinities are computed directly—not as a function of asymmetric conditionals like p_{ij} —using two hyperparameters that control the distance between points in the embedding. Notably, q_{ij} is not normalized across all data, unlike the similar term in t-SNE.

Parametric UMAP [SMG21] is a variation of UMAP whereby a neural network is trained to map high dimensional points to lower dimension. The embedding loss function is adapted from UMAP such that the network learns to position points in a manner similar to using UMAP directly. The formulation of UMAP—using negative sampling and normalization of pairwise relationships across all embedding points—makes it particularly suitable for a neural network variation. The trained parametric model could readily be used to reduce the dimensionality of out-of-sample data that was not used for training.

3 Method

We’re interested in visualizing the penultimate layer representations of adversarial inputs relative to non-adversarial inputs. At this layer the representations are typically high dimensional, and thus we

Algorithm 1 POP- N Score

inputs:
 Z N -dimensional projected representations for correctly classified inputs X
 Y Labels for correctly classified inputs X
 Z^{adv} N -dimensional projected representations for n adversarially perturbed inputs X^{adv}
 Y^{adv} Predicted labels for n adversarially perturbed inputs X^{adv}

```
1: function SCORE
2:   MODEL  $\leftarrow$  TRAIN( $Z, Y$ )            $\triangleright$  train nearest neighbor classifier on  $Z$  and  $Y$ 
3:    $c \leftarrow 0$                           $\triangleright$  initialize preserved prediction counter
4:   for  $i \leftarrow 1, \dots, n$  do        $\triangleright$  loop over adversarial data
5:     if  $Y_i^{adv} = \text{MODEL}(Z_i^{adv})$  then  $\triangleright$  check if prediction is preserved
6:        $c \leftarrow c + 1$                   $\triangleright$  increment counter
7:     end if
8:   end for
9:   return  $c/n$                             $\triangleright$  return preserved prediction rate
10: end function
```

need to project the data to two dimensions for visualization. We propose and define POP- N scoring, a technique that can be used to evaluate the effectiveness of dimensionality reduction in the context of visualizing penultimate layer representations of adversarial images. We then describe how to generate the visualizations.

3.1 POP- N Score

We’d like to generate visualizations from penultimate layer representations of 1) correctly classified inputs and 2) adversarial inputs. We need to project the data to two dimensions for visualization in a scatter plot. To compare dimensionality reduction algorithms for this task, we devised the POP- N score—named as an acronym for *preserving output predictions* in N dimensions—for measuring how well the projected adversarial data preserves the corresponding adversarial output predictions from the underlying model.

Because the representations under consideration are from the penultimate layer of a neural network, we utilize class label predictions—which are from the *neighboring* layer—to evaluate whether the low dimensional embeddings preserve the *expected* structure in the data. We score a projection by whether the non-adversarial nearest neighbors of adversarial points have the same predicted class. The algorithm is illustrated in Figure 1 and described in Algorithm 1.

3.2 Visualization

For visualizing adversarially perturbed data, POP-2 can be used to 1) evaluate the suitability of a specific dimensionality reduction algorithm and/or 2) compare scores across an assortment of algorithms. Once an algorithm is selected, the projected 2D representations can be visualized on a scatter plot. We follow the approach of [LZS20], where projected adversarial representations are visualized alongside projected non-adversarial representations.

4 Experimental Results

In this section we 1) compare POP-2 scores across dimensionality reduction algorithms and adversarial attacks, and 2) generate corresponding visualizations. Hyperparameter selection was performed arbitrarily; we did not conduct hyperparameter optimization and did not focus on manually tuning hyperparameters. For the purpose of our experiments, it was sufficient to have 1) a model that performed well (i.e., not necessarily optimal), 2) an assortment of adversarial attacks that worked well (i.e., haven’t been tuned for maximal effectiveness), and 3) a variety of dimensionality reduction algorithms.

4.1 Experimental Settings

Experiments were conducted using the CIFAR-10 dataset [Kri09], comprised of 60,000 32×32 RGB images across 10 classes, split into 50,000 training images and 10,000 testing images. With pixel values scaled by $1/255$ to be between 0 and 1, we trained an 18-layer, 11,173,962 parameter neural network classifier with a ResNet-inspired architecture¹. Training was conducted for 100 epochs using Adam [KB14] for optimization, with random horizontal flipping and random crop sampling—on images padded with 4 pixels per edge. This resulted in 92.76% accuracy on the test dataset.

4.1.1 Adversarial Attacks

We used the `cleverhans` library [PFC⁺18] to generate untargeted adversarial attacks on the 9,276 correctly classified test images. Attacks were generated using FGSM, BIM, and CW, with an L_2 norm distance metric used for CW. The perturbed images were clipped between 0 and 1 for all attacks and quantized to 256 discrete values for FGSM and BIM. Quantization limits the space of perturbed images to those that could be represented in 24-bit RGB space, but was problematic for CW, where the perturbations are small enough that quantizing essentially reverts the attack². For FGSM, we used $\epsilon = 3/255$, which corresponds to a maximum perturbation of 3 intensity values for each pixel on the unnormalized data. Model accuracy after attack—on the 9,276 attacked images—was 17.2% (i.e., the attack success rate was 82.8%). For BIM, we used 10 iterations with $\alpha = 1/255$ and the maximum perturbation magnitude clipped to $\epsilon = 3/255$. This corresponds to a maximum perturbation of 1 unnormalized intensity value per pixel on each step, ultimately clipped to a maximum perturbation of 3. Accuracy after attack was 0.5%. For CW, we used the default parameters—a learning rate of 0.005, 5 binary search steps, and 1,000 maximum iterations. Accuracy after attack was 0.0%.

Figure 2 shows examples of adversarially perturbed images across the attacks utilized for our experiments. Images were chosen as the first of their class from the 9,276 correctly classified test images.

4.1.2 Dimensionality Reduction

For the network architecture we used, the penultimate layer representations are comprised of 512 values formed as the output of a global average pooling operation. For projecting the corresponding representations to two dimensions, we use PCA, t-SNE, UMAP, and parametric UMAP. We do not tune hyperparameters, and we keep the defaults as specified by the libraries we utilized, `scikit-learn` [PVG⁺11] and `umap-learn` [MHSG18]. All considered algorithms include pseudo-randomness, including PCA, for which `randomize SVD` is automatically chosen as the SVD solver.

¹We follow the ResNet-18 architecture of [kua], which differs in filter counts and depth relative to the ResNet-20 architecture used for CIFAR-10 in the original ResNet paper [HZRS16].

²[CW17] addresses this issue through a greedy search process that restores attack quality by changing one pixel value at a time. We did not utilize that approach for our experiments.



Figure 2: Example CIFAR-10 images after adversarial perturbation. The leftmost column shows the original image, followed by three columns corresponding to FGSM, BIM, and CW attacks, respectively. Images were chosen as the first of their class from the set of—correctly classified without perturbation—test images.

Table 1: Average POP-2 scores plus/minus the sample standard deviation, calculated across 100 trials that each uses a different seed for 2D dimensionality reduction. Rows are sorted in descending order by the mean score across attacks. For each attack, the highest POP-2 score is in bold. *OOS* is used for labeling the out-of-sample approaches.

Dimensionality Reduction	Adversarial Attack		
	FGSM	BIM	CW
UMAP	0.8622 \pm 0.0047	0.9950 \pm 0.0004	0.3467 \pm 0.0065
Parametric UMAP	0.8589 \pm 0.0114	0.9901 \pm 0.0056	0.3365 \pm 0.0116
t-SNE	0.8554 \pm 0.0024	0.9948 \pm 0.0005	0.2144 \pm 0.0027
OOS parametric UMAP	0.8188 \pm 0.0105	0.9765 \pm 0.0094	0.2625 \pm 0.0173
PCA	0.2903 \pm 0.0000	0.4062 \pm 0.0000	0.1966 \pm 0.0000
OOS PCA	0.2891 \pm 0.0000	0.3767 \pm 0.0000	0.2056 \pm 0.0000
OOS UMAP	0.1592 \pm 0.0402	0.1383 \pm 0.0345	0.1202 \pm 0.0377

We use two approaches for mapping high dimensional representations to 2D. For the first, model fitting and data transformation are coupled. Non-adversarial representations R are combined with adversarial representations R^{adv} and the data is jointly projected to 2D. For the second approach—limited to dimensionality reduction algorithms that support out-of-sample projection—we fit models using only non-adversarial representations R , producing a transformation function that is used for projecting both R and R^{adv} . A benefit to utilizing the latter approach is that it more readily permits a comparison of visualizations across attacks since the non-adversarial projections are held constant.

4.2 POP-2 Scores

We calculate POP-2 scores across the adversarial attacks and dimensionality reduction algorithms. The results are reported on Table 1, where the values are averaged across 100 trials, each using a different seed for dimensionality reduction.

4.3 Visualizations

Figure 3 shows example visualizations generated using UMAP for dimensionality reduction, comparing the adversarial projections across the first three classes. Figure 4 shows example visualizations generated using out-of-sample parametric UMAP for dimensionality reduction, comparing adversarial airplane (selected as the dataset’s first class) projections across the three attacks.

4.4 Hardware and Software

All experiments were conducted on a desktop computer with Ubuntu 20.10, using Python 3.9. The hardware includes an AMD Ryzen 7 2700X CPU, 64GB of memory, and an NVIDIA TITAN RTX GPU with 24GB of memory. The GPU was utilized for training the neural network and generating adversarial attacks.

The code used for running the experiments is available at <https://github.com/dstein64/vrapi>.

5 Discussion

5.1 POP-2 Scores

As shown in Table 1, the UMAP algorithm corresponded to the maximum average POP-2 score for each of the attacks considered. The scores for BIM were highest, which is interesting particularly relative to the lower scores for FGSM, given the relationship between those algorithms. Notably, the CW scores are lowest, suggesting there may be issues with using the POP-2 metric with that attack. We discuss this further in Section 7.

The variability across trials was minor, as shown by the reported standard deviations. Out-of-sample UMAP had the highest variability and also the lowest scores, making it particularly unsuitable for this problem.

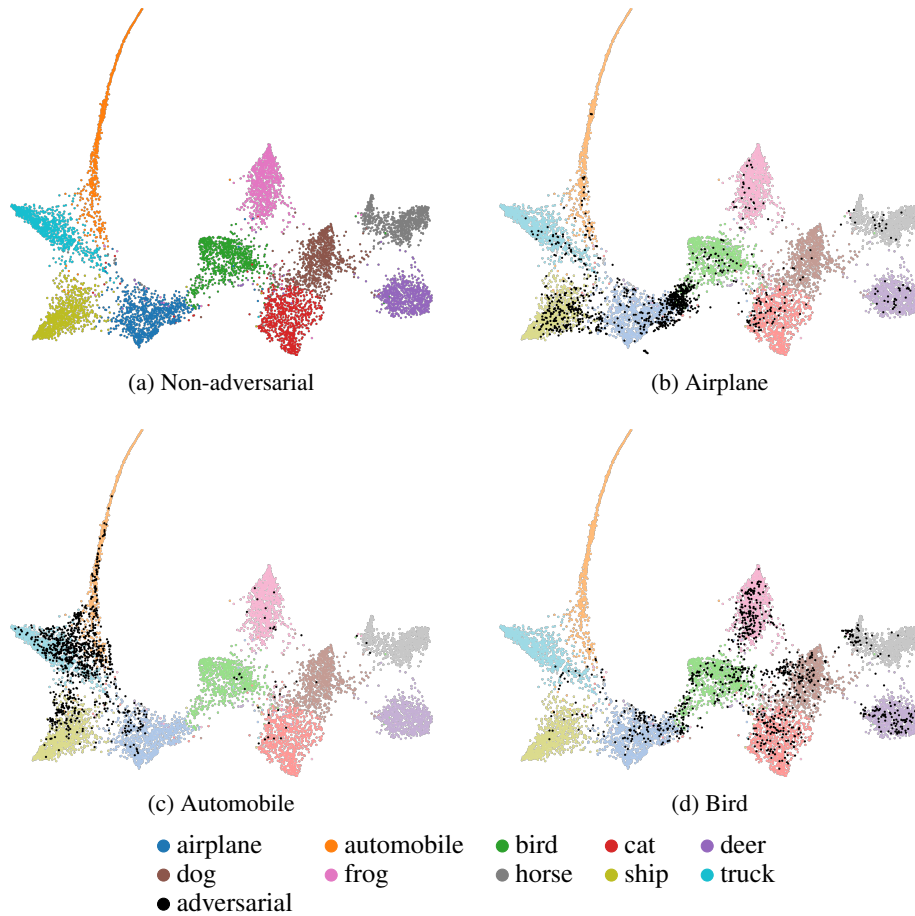


Figure 3: Visualizations of CIFAR-10 test data penultimate layer representations, projected to two dimensions with UMAP. (a) shows only the projected representations of non-adversarial data. (b), (c), and (d) show faded non-adversarial points along with black points corresponding to FGSM adversarially perturbed airplanes, automobiles, and birds, respectively.

For each adversarial input, the POP- N score considers the class of the closest non-adversarial point in the space of representation projections. An alternative formulation of POP- N scoring could hypothetically use nearest class centroids in place of nearest neighbors. In such a scenario, line 2 of Algorithm 1 would train a nearest centroid classifier instead of a nearest neighbor classifier. We intentionally avoided this approach because it would not properly accommodate 1) projections with multiple clusters per class, 2) non-spherical class clusters, and 3) unevenly sized class clusters.

5.2 Visualizations

Non-adversarial data One of the first patterns we noticed was in the structure of the non-adversarial data. In Figures 3 and 4, and other plots we inspected, the data are organized in clusters that are systematically arranged, as has been often found in visualizations of hidden unit representations. Each class forms its own cluster, with the set of vehicle clusters on one side and animal clusters on the other side, joined by the two aerial classes, airplane and bird.

Comparing classes Figure 3 shows the differences in projected representations of attacked inputs for an assortment of classes. It is noticeable how each class of attacked image is unique in the general way its projected representations manifest. For example, many of the points for the adversarially perturbed airplanes are concentrated in the region connecting airplane and bird clusters. For the adversarially perturbed automobiles, a large portion of the projections appear to uniformly fill the truck cluster. The bird class’s projected representations are spread most widely.

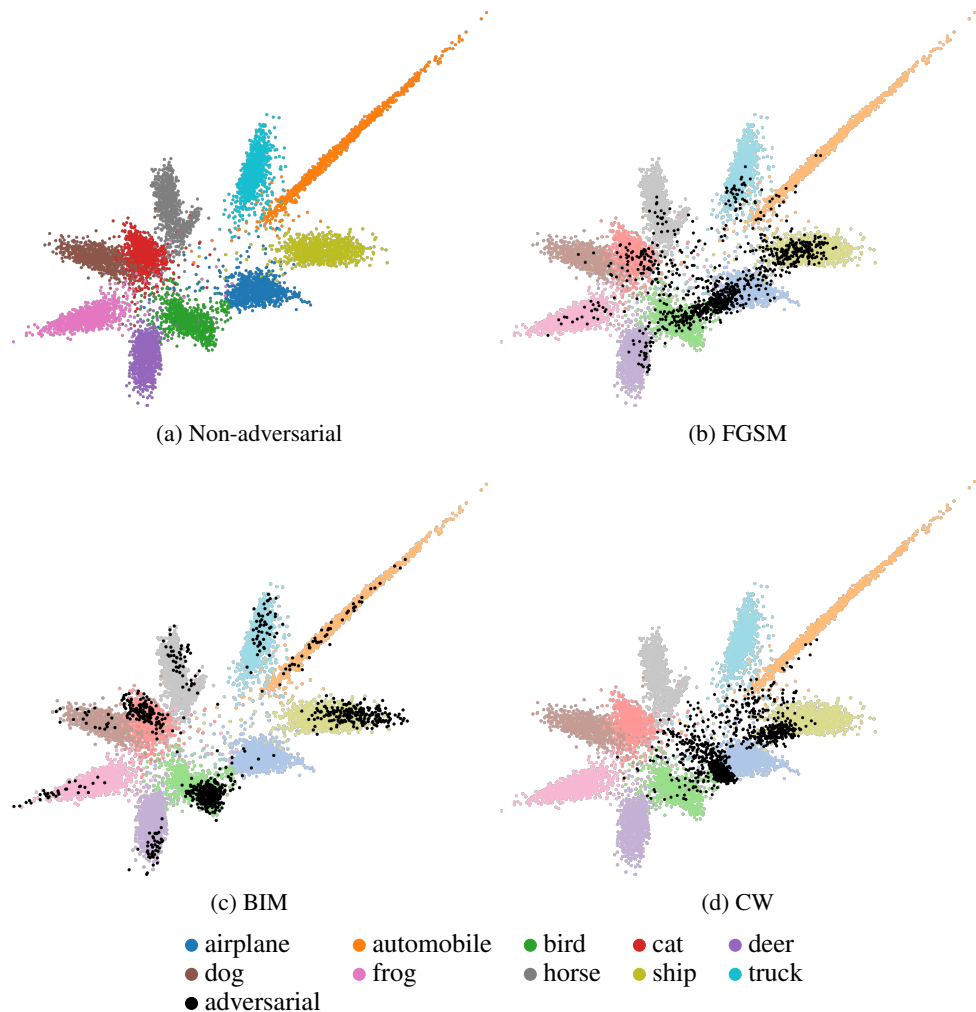


Figure 4: Visualizations of CIFAR-10 test data penultimate layer representations, projected to two dimensions with out-of-sample parametric UMAP. (a) shows only the projected representations of non-adversarial data. (b), (c), and (d) show faded non-adversarial points along with black points corresponding to FGSM, BIM, and CW adversarially perturbed airplanes, respectively.

Comparing attacks On Figure 4 we can see the differences in projected representations for the adversarially perturbed airplanes across the different attacks. Comparing FGSM and BIM, it appears that the representations for adversarial inputs are occupying different regions of each class’s representation space. For example, low dimensional representations for the FGSM adversarially perturbed airplane images occupy the leftmost portion of the ship cluster, whereas the corresponding points for BIM occupy the rightmost portion. For CW, it’s noticeable how the points for adversarially perturbed airplane inputs are concentrated slightly outside the airplane cluster. This may be reflective of the minor magnitude of the CW perturbation distance. It’s also noticeable that a non-negligible amount of adversarial density occupies a region of the embedding—above the airplane cluster—that is sparse for non-adversarial data. This was not the case for FGSM and BIM attacks.

6 Related Work

Grand Tour Work similar to ours is presented in [LZS20], where one of the example use cases for the proposed Grand Tour visualization technique is in the context of adversarial examples. They show how Grand Tour can be used to visualize the layer-by-layer behavior of adversarial image representations for MNIST images. In addition to showing the dynamics throughout different

layers, they also visualize how representations change as a function of the optimization process used for generating an adversarial image. Some aspects that distinguish our work from theirs include 1) proposing a metric for evaluating visualizations, 2) using the CIFAR-10 dataset as opposed to MNIST, 3) considering an assortment of dimensionality reduction techniques—both linear and non-linear, in contrast to Grand Tour, which is “fundamentally a linear method”—for visualizing adversarial perturbations, 4) including more points in our visualizations, 5) focusing on untargeted adversarial attacks instead of targeted attacks, and 6) considering an assortment of adversarial attacks.

Adversarial attack visualizations More broadly, there are various works that use visualizations as a way to better understand adversarial attacks. [XLZ⁺19] proposes a technique for image-level interpretability of adversarial examples, whereby class activation maps and perturbation information are overlaid on original and adversarially attacked images. [NQ17] describes Adversarial-Playground, an interactive web application that shows original images alongside adversarial counterparts, intended to help users visually explore the behavior of adversarial attacks and how they impact their targeted classifiers. In addition to displaying—original and adversarial—images themselves, visualizations of decision boundaries have been another technique used to understand classifier vulnerability to adversarial inputs. For example, [LCLS17] presents such visualizations—see Figures 3, 4, and 5 in that paper—as part of their research on adversarial example transferability.

7 Conclusion

The POP-2 score can be used to evaluate dimensionality reduction algorithms under the context of visualizing representations of adversarially perturbed inputs. We showed how this can be used to compare algorithms and/or check the performance of a specific algorithm. Experiments indicate that there is a wide difference in effectiveness across different dimensionality reduction algorithms and adversarial attacks.

The research leaves open unanswered questions, suggesting various avenues for future work. The POP-2 metric was devised with specific consideration for representations from the penultimate layer of neural networks. Devising metrics for earlier layers would permit a quantitative evaluation of dimensionality reduction techniques on such layers. In the absence of a method for quantifying performance in earlier layers, the representations could be visualized using the same dimensionality reduction algorithms that scored high for the penultimate layer, but there would be more uncertainty regarding the visualization accuracy³. Finally, future work could additionally address the low POP-2 scores for the CW attack, exploring why this occurs and either 1) devising a metric that would potentially be more suitable than POP-2 for that attack, or 2) searching for or developing alternative dimensionality reduction algorithms that would potentially be more applicable for that attack.

8 Broader Impact

Visualizing the representations of adversarially perturbed images contributes to a further understanding of 1) neural networks and 2) adversarial attacks and defenses against neural networks. While this knowledge could conceivably be utilized by a malicious actor, we believe the potential benefits provided by this area of research outweigh the potential for misuse.

³The term “accuracy” is used loosely here, as it’s not well defined in this context.

References

- [AM18] Naveed Akhtar and Ajmal Mian. Threat of Adversarial Attacks on Deep Learning in Computer Vision: A Survey. *arXiv:1801.00553 [cs]*, February 2018. 1
- [BPV⁺04] Yoshua Bengio, Jean-françois Paiement, Pascal Vincent, Olivier Delalleau, Nicolas L. Roux, and Marie Ouimet. Out-of-Sample Extensions for LLE, Isomap, MDS, Eigenmaps, and Spectral Clustering. In *Advances in Neural Information Processing Systems 16*, pages 177–184. MIT Press, 2004. 2
- [CW17] Nicholas Carlini and David Wagner. Towards Evaluating the Robustness of Neural Networks. *arXiv:1608.04644 [cs]*, March 2017. 2, 5
- [GSS15] Ian Goodfellow, Jonathon Shlens, and Christian Szegedy. Explaining and Harnessing Adversarial Examples. In *International Conference on Learning Representations, 2015*. 2
- [HZRS16] Kaiming He, Xiangyu Zhang, Shaoqing Ren, and Jian Sun. Deep Residual Learning for Image Recognition. In *2016 IEEE Conference on Computer Vision and Pattern Recognition (CVPR)*, pages 770–778, June 2016. 5
- [KB14] Diederik Kingma and Jimmy Ba. Adam: A Method for Stochastic Optimization. *arXiv:1412.6980 [cs]*, December 2014. 5
- [KGB17] Alexey Kurakin, Ian Goodfellow, and Samy Bengio. Adversarial examples in the physical world. *arXiv:1607.02533 [cs, stat]*, February 2017. 1, 2
- [Kri09] Alex Krizhevsky. Learning Multiple Layers of Features from Tiny Images. Technical report, 2009. 5
- [kua] kuangliu. kuangliu/pytorch-cifar. <https://github.com/kuangliu/pytorch-cifar>. 5
- [LCLS17] Yanpei Liu, Xinyun Chen, Chang Liu, and Dawn Song. Delving into Transferable Adversarial Examples and Black-box Attacks. *arXiv:1611.02770 [cs]*, February 2017. 9
- [LZS20] Mingwei Li, Zhenge Zhao, and Carlos Scheidegger. Visualizing neural networks with the grand tour. *Distill*, 2020. <https://distill.pub/2020/grand-tour>. 4, 8
- [MHM20] Leland McInnes, John Healy, and James Melville. UMAP: Uniform Manifold Approximation and Projection for Dimension Reduction. *arXiv:1802.03426 [cs, stat]*, September 2020. 3
- [MHSG18] Leland McInnes, John Healy, Nathaniel Saul, and Lukas Grossberger. Umap: Uniform manifold approximation and projection. *The Journal of Open Source Software*, 3(29):861, 2018. 5
- [MLW⁺18] Xingjun Ma, Bo Li, Yisen Wang, Sarah M. Erfani, Sudanthi Wijewickrema, Grant Schoenebeck, Dawn Song, Michael E. Houle, and James Bailey. Characterizing Adversarial Subspaces Using Local Intrinsic Dimensionality. *arXiv:1801.02613 [cs]*, March 2018. 1
- [MMS⁺19] Aleksander Madry, Aleksandar Makelov, Ludwig Schmidt, Dimitris Tsipras, and Adrian Vladu. Towards Deep Learning Models Resistant to Adversarial Attacks. *arXiv:1706.06083 [cs, stat]*, September 2019. 1
- [NQ17] Andrew P. Norton and Yanjun Qi. Adversarial-Playground: A Visualization Suite Showing How Adversarial Examples Fool Deep Learning. *arXiv:1708.00807 [cs]*, August 2017. 9
- [Pea01] Karl Pearson. LIII. On Lines and Planes of Closest Fit to Systems of Points in Space. *Philosophical Magazine Series 6*, 2(11):559–572, November 1901. 3
- [PFC⁺18] Nicolas Papernot, Fartash Faghri, Nicholas Carlini, Ian Goodfellow, Reuben Feinman, Alexey Kurakin, Cihang Xie, Yash Sharma, Tom Brown, Aurko Roy, Alexander Matyasko, Vahid Behzadan, Karen Hambardzumyan, Zhishuai Zhang, Yi-Lin Juang, Zhi Li, Ryan Sheatsley, Abhibhav Garg, Jonathan Uesato, Willi Gierke, Yinpeng Dong, David Berthelot, Paul Hendricks, Jonas Rauber, and Rujun Long. Technical report on the cleverhans v2.1.0 adversarial examples library. *arXiv preprint arXiv:1610.00768*, 2018. 5
- [PVG⁺11] F. Pedregosa, G. Varoquaux, A. Gramfort, V. Michel, B. Thirion, O. Grisel, M. Blondel, P. Prettenhofer, R. Weiss, V. Dubourg, J. Vanderplas, A. Passos, D. Cournapeau, M. Brucher, M. Perrot, and E. Duchesnay. Scikit-learn: Machine learning in Python. *Journal of Machine Learning Research*, 12:2825–2830, 2011. 5

- [SMG21] Tim Sainburg, Leland McInnes, and Timothy Q. Gentner. Parametric UMAP embeddings for representation and semi-supervised learning. *arXiv:2009.12981 [cs, q-bio, stat]*, April 2021. 3
- [SZS⁺14] Christian Szegedy, Wojciech Zaremba, Ilya Sutskever, Joan Bruna, Dumitru Erhan, Ian Goodfellow, and Rob Fergus. Intriguing properties of neural networks. In *International Conference on Learning Representations*, 2014. 1
- [TV16] Pedro Tabacof and Eduardo Valle. Exploring the Space of Adversarial Images. *arXiv:1510.05328 [cs]*, June 2016. 1
- [vdMH08] Laurens van der Maaten and Geoffrey Hinton. Visualizing Data Using t-SNE. *Journal of Machine Learning Research*, 9(Nov):2579–2605, 2008. 3
- [XLZ⁺19] Kaidi Xu, Sijia Liu, Gaoyuan Zhang, Mengshu Sun, Pu Zhao, Quanfu Fan, Chuang Gan, and Xue Lin. Interpreting Adversarial Examples by Activation Promotion and Suppression. *arXiv:1904.02057 [cs]*, September 2019. 1, 9